REPORT DOCUMENTATION PAGE

Form Approved
OMB No. 0704-0188

1. REPORT DATE *(DD-MM-YYYY)*	2. REPORT TYPE	3. DATES COVERED *(From - To)*
02-08-2010	FINAL	01-Feb-09 – 28-Feb-10

4. TITLE AND SUBTITLE

Chemical synthesis of next generation high energy product hybrid SmCo permanent magnets for high temperature applications

5a. CONTRACT NUMBER

5b. GRANT NUMBER
N00014-09-1-0590

5c. PROGRAM ELEMENT NUMBER

6. AUTHOR(S)
Vincent Harris

5d. PROJECT NUMBER

5e. TASK NUMBER

5f. WORK UNIT NUMBER

7. PERFORMING ORGANIZATION NAME(S) AND ADDRESS(ES)

Northeastern University
360 Huntington Avenue, 960RP
Boston, MA 02115

8. PERFORMING ORGANIZATION REPORT NUMBER

FINAL

9. SPONSORING / MONITORING AGENCY NAME(S) AND ADDRESS(ES)
Office of Naval Research
875 North Randolph St.
Arlington, VA 02115-5000

10. SPONSOR/MONITOR'S ACRONYM(S)
ONR

11. SPONSOR/MONITOR'S REPORT NUMBER(S)

12. DISTRIBUTION / AVAILABILITY STATEMENT

Approved for Public Release, distribution is Unlimited

13. SUPPLEMENTARY NOTES

14. ABSTRACT

High performance permanent magnets, i.e. those having appreciable energy products, can be broadly classified into three categories: rare earth-3d transition metal intermetallics ($Nd_2Fe_{14}B$, Sm_1Co_5 and Sm_2Co_{17}), AlNiCo (alloys composed primarily of iron with additions of aluminum, nickel, cobalt, copper and sometimes titanium) and ceramic magnets (typically strontium-doped barium hexaferrites). The magnets containing rare earth elements provide the highest energy products, $(BH)_{max}$, but are expensive and prone to corrosion and, as such, pose severe cost limitations as well as supply chain challenges to commercial industries. Very few major developments in viable permanent magnet materials have occurred since the development of Nd–Fe–B in the early 1980s. Here, we report a ferromagnetic material based upon nanoscale cobalt carbide particles that provide a rare-earth free alternative to high performance permanent magnets. The cobalt carbide-based magnets described herein are processed by chemical polyol reduction of metal salts. Packaging may be in the form of isotropic or anisotropic high density compacts, bonded magnets, particle suspensions, etc. The best properties of the carbide particles of this work include room temperature coercivities greater than 3.4 kOe and room temperature saturation magnetization up to 73 emu g^{-1}.

15. SUBJECT TERMS
Permanent magnets, cobalt carbide, nanoparticles

16. SECURITY CLASSIFICATION OF:			17. LIMITATION OF ABSTRACT	18. NUMBER OF PAGES	19a. NAME OF RESPONSIBLE PERSON
a. REPORT	b. ABSTRACT	c. THIS PAGE			Vincent Harris
UUUU	UUUU	UUUU		12	19b. TELEPHONE NUMBER *(include area code)* 617-373-7603

Contract Information

Contract Number	N00014-09-1-0590
Title of Research	Chemical synthesis of next generation high energy product hybrid SmCo permanent magnets for high temperature applications
Principal Investigator	Vincent Harris
Organization	Northeastern University

Technical Section

Technical Objectives

High performance permanent magnets, i.e. those having appreciable energy products, can be broadly classified into three categories: rare earth-3d transition metal intermetallics ($Nd_2Fe_{14}B$, Sm_1Co_5 and Sm_2Co_{17}), AlNiCo (alloys composed primarily of iron with additions of aluminum, nickel, cobalt, copper and sometimes titanium) and ceramic magnets (typically strontium-doped barium hexaferrites). Commercial permanent magnet applications include those for exerting attractive and repelling forces (e.g. magnetic separators, latches, torque drives, bearings, etc), energy conversion (e.g. magnetos, generators, alternators, eddy current brakes, motors and actuators), directing and shaping particle beams and electromagnetic waves (cathode ray tubes, travelling wave tubes, klystrons, cyclotrons, ion pumps, etc) and providing magnetic bias fields for a wide range of RF, microwave and millimeter-wave devices (isolators, circulators, phase shifters, filters, etc). The magnets containing rare earth elements provide the highest energy products, $(BH)_{max}$, but are expensive and prone to corrosion and, as such, pose severe cost limitations as well as supply chain challenges to commercial industries. Alternatively, AlNiCo and ceramic magnets have substantially lower $(BH)_{max}$ values but are significantly less expensive and more readily available from many sources. For that reason AlNiCo and ceramic ferrite have defined substantial global permanent magnet market segments. In the case of ceramic magnets the annual revenue generated is second only to Nd–Fe–B. Very few major developments in viable permanent magnet materials have occurred since the development of Nd–Fe–B in the early 1980s. One such development, Zr–Co–B by Ghemawat *et al.* [1], has not experienced further commercial development owing to materials costs. Similarly, AlNiCo and ceramic magnets have not experienced significant improvement in permanent magnet properties for several decades. Here, we report a ferromagnetic material based upon nanoscale cobalt carbide particles that provide a rare-earth free alternative to high performance permanent magnets. The cobalt carbide-based magnets described herein are processed by chemical polyol reduction of metal salts. The precipitate of the reaction need only be rinsed and dried prior to packaging. Packaging may be in the form of isotropic or anisotropic high density compacts, bonded magnets, particle suspensions, etc. The best properties of the carbide particles of this work include room temperature coercivities greater than 3.4 kOe and room temperature saturation magnetization up to 73 emu g^{-1}.

Technical Approach

I. Introduction

Rare earth–transition metal (RE-TM) compounds with iron or cobalt as the TM constituent and one of the magnetic light REs, i.e., Pr, Nd, or Sm, as the RE constituent are especially well-suited for use as high-temperature, high performance permanent magnets. [2–13] In the RE-TM intermetallic compounds, the RE unpaired 4*f* electrons provide the magnetocrystalline anisotropy, which is potentially much stronger than the shape anisotropy, whereas the TM 3*d* electrons provide most of the magnetization and determine the Curie temperature. The Sm–Co binary equilibrium phase diagram indicates seven intermetallic compounds (RE:TM ratios 2:17, 1:5, 2:7, 1:3, 1:2, 9:4, and 3:1) that are stable under standard atmospheric conditions. Among these, $SmCo_5$ and Sm_2Co_{17} are the most important permanent magnetic materials in the SmCo system. Both $SmCo_5$ and Sm_2Co_{17} materials adopt hexagonal close packed (hcp) structures where Co dumbbell ion pairs are present in alternating layers along the crystallographic *c* axis. The easy magnetization direction of these SmCo intermetallic compounds is along the *c* axis and the room temperature magnetocrystalline anisotropy constant is of the order of 10^8 erg/cm^3. [4] Furthermore, these compounds exhibit a very high Curie temperature (T_c=1020 K), which makes them superior to other classes of permanent magnetic materials, such as FePt (T_c=750 K) and $Nd_2Fe_{14}B$ (T_c=585 K), for high-temperature applications. However, the high reactivity of SmCo nanoparticles renders them prone to rapid oxidation, making the synthesis of nanostructured $SmCo_5$ extremely difficult. Until now, two standard processing methods, i.e., ball milling and melt spinning, have been employed in the fabrication of nanostructured $SmCo_5$ magnets. However, these techniques provide limited control of the size and shape of the final magnetic particles. Solution-phase chemical synthesis approaches have been applied to the preparation of monodispersed magnetic nanoparticles [14] and have been extended to the synthesis of $SmCo_5$ nanoparticles. Specifically, by coupling the reduction of samarium acetylacetonate, $Sm(acac)_3$, with the thermal decomposition of cobalt carbonyl, $Co_2(CO)_8$, SmCo particles were formed. [15] In Ref. 15, Sm and Co were demonstrated to possess the appropriate 1:5 molar ratio; however, there was no conclusive evidence that the hcp-structured $SmCo_5$ phase was formed nor were hard magnetic properties confirmed at room temperature. Recently $SmCo_5$ was synthesized by high-temperature reductive annealing of core/shell-structured Co/Sm_2O_3 nanoparticles [16] at temperatures between 900 and 1100 °C under an inert atmosphere in the presence of metallic Ca and KCl. This calciothermic co-reduction process is similar to the synthesis of bulk $SmCo_5$. [4] The direct chemical synthesis of SmCo-based nanoparticles exhibiting high coercivity has been a long standing goal for the magnetic materials community due to potential applications of these nanomagnets as high performance permanent magnets and, most importantly, for their potential as aligned exchange-coupled nanocomposite magnets. [17,18]

Here, we report a ferromagnetic material based upon nanoscale cobalt carbide particles that provide a rare-earth free alternative to high performance permanent magnets. The cobalt carbide-based magnets described herein are processed by

chemical polyol reduction of metal salts. The precipitate of the reaction need only be rinsed and dried prior to packaging. Packaging may be in the form of isotropic or anisotropic high density compacts, bonded magnets, particle suspensions, etc. The best properties of the carbide particles of this work include room temperature coercivities greater than 3.4 kOe and room temperature saturation magnetization up to 73 emu g^{-1}. Further, there is a clear dependence upon processing conditions in which the tendency to increase coercivity varies inversely with saturation magnetization. The highest room temperature $(BH)_{max}$, the primary figure of merit for permanent magnets, is >20 kJm^{-3} for free (i.e. not compacted) carbide powders. This value has not yet been optimized for composition and processing but nonetheless compares favourably with both AlNiCo and ceramic magnets as free powders, making these carbide particles a potentially viable and competitive room temperature permanent magnet material.

There has been much attention paid to carbon-containing magnetic materials, which have many potential applications such as in high-density magnetic recording media, high resistivity soft magnetic materials, magnetic toner in xerography and as contrast agents in high resolution magnetic resonance imaging. In previous work, researchers have focused on cobalt/carbide related materials which include carbon-coated magnetic-metal nanocrystallites [19], Co–C granular films [20-23], M_nC (M = Fe, Co, Ni, Cu, n = 1–6) nanoclusters [24] and Co_2C films [25]. In those earlier works, the focus was on the fabrication and application of carbon-related composites. The granular magnetic films, consisting of isolated particles suspended in a nonmagnetic host, were expected to produce low noise high-density magnetic media. The so-called core–shell nanoparticles constitute another form of nanocomposite. In the 1990s, McHenry *et al.* reported on the magnetic properties of carbon coated cobalt nanocrystallites [26]. These nanocrystallites were proposed for applications ranging from recording media to emerging biomedical applications in imaging and cancer remediation therapies. Additional research includes theoretical and experimental studies of M_nC (M = Fe, Ni, Co, etc.) clusters [27], which are cage-like structures of transition metal containing carbon atoms, that demonstrate unusual structural and chemical stabilities; these studies, however, did not explore, nor report, magnetic properties.

This study follows earlier work by Chinnasamy *et al.* [28] that proposed the direct precipitation of SmCo metallic particles using similar chemical paths put forth here. Since that time authors of this publication have determined that the principal phase(s) of the precipitate of [28] were in fact majority carbide phases, although the existence of nanostructured or amorphous SmCo cannot be ruled out. A recent publication that followed processing paths similar to [28], and those put forth here, have also proposed SmCo as the principal product [29]. Published x-ray diffraction (XRD) data of [28, 29] are markedly similar and suggest carbide phases (i.e. Co_2C) as their principal products. This work focuses on expanding the understanding of processing conditions that optimize phase purity, structure and magnetic properties of carbide nanoparticles.

II. Chemical processing and experimental procedures

The chemical synthesis methods employed here to produce size-, shape-, composition- and phase-controlled, highly coercive cobalt carbide nanoparticles are based upon reduction of metallic salts in a liquid polyol medium that acts as both a solvent and a reducing agent. The reduction reaction kinetics of the process are

enhanced by controlling the type, temperature and concentration of the polyol medium and by adding appropriate surfactants that limit the oxidation of ions when reduced and regulate the growth of particles as the reaction progresses. The chemical synthesis includes adding 0.1–0.2M concentration of Co (II) acetate to tetraethylene glycol. Poly-vinylpyrrolidone (PVP, MW ~ 40,000) was introduced as a capping agent along with NaOH and Sm (III) acetate as catalysts. The solution was allowed to degas in N_2 gas (or in some instances Ar gas) for 10–15 min prior to the start of the reaction. The solution was then heated to the boiling point of tetraethylene glycol (~573 K) for 1–2 h using a distillation apparatus with magnetic stirring. After the completion of the reaction, the solution was cooled to room temperature, magnetically separated several times using an external rare earth magnet and rinsed repeatedly in methanol to remove unreacted catalyst. It is noteworthy that Sm-based by-products were reduced to below detection limits of energy dispersive x-ray spectroscopy (EDXS) by these rinsing procedures. The black precipitate was dried under vacuum at room temperature prior to characterization.

The dried powders were characterized by XRD, transmission electron microscopy (TEM) and vibrating sample magnetometry (VSM) for the determination of phase, morphology and temperature dependent magnetic properties, respectively. XRD measurements were performed using a Rigaku Ultima-III Bragg–Brentano diffractometer employing Cu-Kα radiation (λ = 0.15418 nm) in the θ–2θ powder diffraction geometry. Thermomagnetometry was performed using a Lakeshore Cryotonics Inc. Model 7400 VSM for temperatures ranging from room temperature to 1000 K. A Quantum Design physical property measurement system (PPMS) was employed to extend the temperature studies to 10 K. The powders were characterized using a JEOL 2200-FX high-resolution transmission electron microscope with a 200 kV accelerating voltage. Samples for TEM were prepared by dispersing a drop of nanoparticle-loaded liquid suspension onto a carbon film supported by copper mesh (400 grid mesh) followed by evaporation of the liquid medium. Fast Fourier Transforms (FFTs) and Inverse-Fast Fourier transforms (IFFTs) were obtained from experimental high resolution TEM images using the Digitalmicrograph™ software. EDXS was utilized to determine the composition of the individual powder particles.

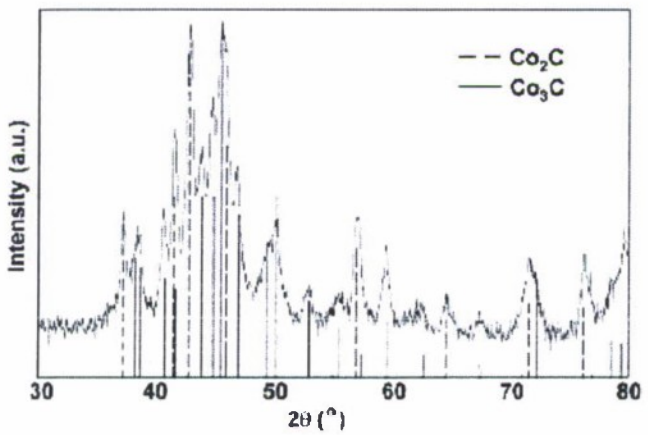

Figure 1 A representative θ–2θ XRD scan obtained from powders processed using the polyol reduction reaction. Vertical lines corresponding to the position and amplitude of diffraction peaks from JCPDS reference powder diffraction files Co_2C (65-1457) and Co_3C (26-0450) are also presented.

III. Results and discussion

Figure 1 shows a representative θ–2θ XRD scan obtained from powders processed using the polyol reduction method described herein. In figure 1, the data collected at room temperature from powders that were chemically processed, rinsed and dried are

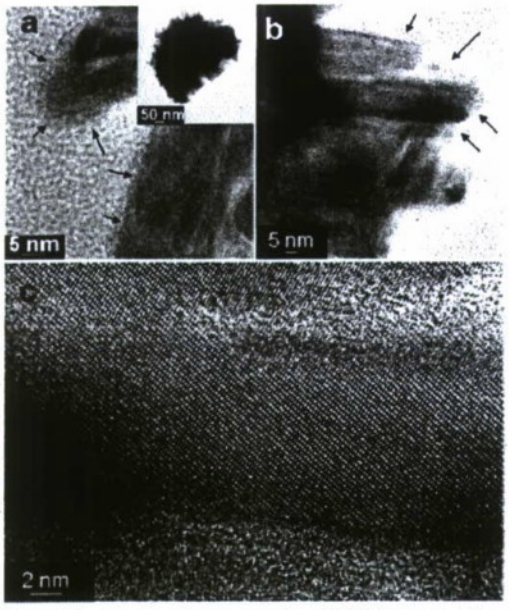

Figure 2 (*a*)–(*c*) High-resolution TEM images of a representative cobalt carbide sample. The inset to (*a*) shows an agglomerated particle cluster about 300–500 nm in diameter. Panels (*a*) and (*b*) are TEM images of rod-like Co-carbide crystals surrounded by a thin 1–4 nm graphite-like layer (denoted by arrows). Figure 2(*c*) is an HRTEM image of a rod-like Co-carbide nanoparticle of aspect ratio near 5 : 1.

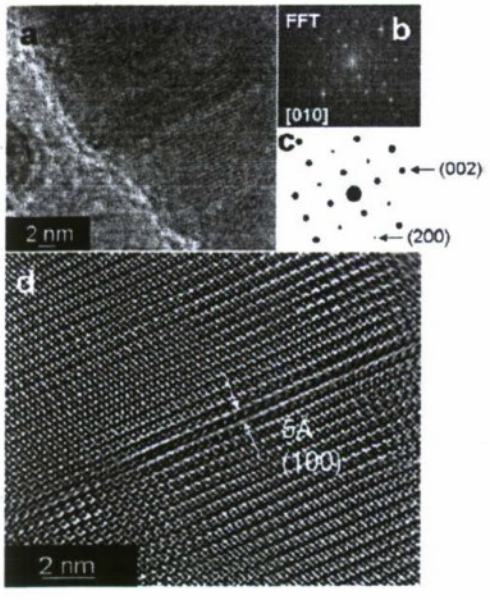

Figure 3 (*a*)–(*c*) HRTEM image of a Co_3C nanoparticle with orientation close to the [0 1 0] zone axis. The FFT (figure 3(*b*)) was indexed to the Co_3C phase (space group: *Pnma* with a = 5.03 Å, b = 6.73Å and c = 4.48 Å) with additional reflections appearing due to double diffraction. A simulated diffraction pattern of Co_3C along this zone axis is provided for comparison in (*c*). The corresponding IFFT image (*d*) shows the lattice spacing of about 5Å, consistent with the [1 0 0] direction along the long axis of the particle.

depicted with an overlay of data from JCPDS reference powder diffraction files Co_2C (65-1457) and Co_3C (26-0450) in which the intensity and the position of each Bragg diffraction peak is represented by a vertical line.

There exist some diffraction features, for example near 67° in 2θ, whose amplitude arises from residual phases that may include different allotropes of carbon and/or unreacted precursors. As yet, residual phases have not been identified; however, these may be related to the apparent surface coating observed in figure 2. XRD analysis confirms that Co_2C and Co_3C are the dominant phases present in these nanoparticles.

Figures 2(*a*)–(*c*) depict high-resolution TEM images. TEM observations show agglomerated particle clusters, about 300–500 nm in diameter (see inset to figure 2(*a*)), consisting of nanocrystalline Co-carbide particles with acicular or rod-like morphology having an approximate 2 : 1 aspect ratio. The ferromagnetic nature of these particles is the driving force behind particle agglomeration. Figures 2(*a*) and (*b*) are TEM images of rod-like Co-carbide crystals. These crystals are surrounded by a thin, 1–4 nm graphite-like layer, denoted by arrows in figures 2(*a*) and (*b*). The graphitic layer appears in these samples as a layered structure and has been previously reported as an 'onion-like' structure in carbide nanoparticles [30]. Such a graphitic layer may form during synthesis from the reduction of precursors and surfactants and may act as a barrier that impedes crystal growth. Figure 2(*c*) is an HRTEM image of a rod-like Co-carbide nanoparticle with an aspect ratio near 5 : 1. In order to determine the crystal structure and preferred growth directions, FFTs were obtained from HRTEM images of individual nanocrystalline particles. Figure 3(*a*) is a HRTEM image of a Co_3C nanoparticle with orientation close to the [0 1 0] zone axis. The FFT seen in figure 3(*b*) was obtained from part of the crystal and indexed to the Co_3C phase (space group: *Pnma* with a = 5.03 Å, b = 6.73Å and c = 4.48 Å) with additional

Table 1. Structural properties determined by XRD and electron diffraction measurements.

Sample no	Volume ratio Co_2C : Co_3C	Lattice parameters of Co_2C (Å)			Lattice parameters of Co_3C (Å)		
		a	*b*	*c*	*a*	*b*	*c*
Bulk standards		4.371	4.446	2.897	4.444	4.993	6.707
SAED		4.37	4.45	2.90	4.48	5.03	6.73
4-4 (2)	1.89 : 1	4.361	4.446	2.888	4.448	5.005	6.718
4-4 (3)	1.06 : 1	4.362	4.444	2.891	4.450	5.002	6.712
4-4 (4)	0.93 : 1	4.365	4.443	2.894	4.454	4.998	6.714
4-4 (5)	0.99 : 1	4.364	4.443	2.900	4.443	5.005	6.710
4-4 (8)	1.46 : 1	4.361	4.444	2.890	4.454	5.004	6.707

reflections appearing due to double diffraction. A simulated diffraction pattern of Co_3C along this zone axis is provided for comparison (see figure 3(*c*)). The corresponding IFFT image (figure 3(*d*)) shows the lattice spacing of about 5Å, consistent with the [1 0 0] direction along the long axis of the particle. Figure 4 shows a HRTEM image of a Co_2C crystal (space group: *Pnnm* with a = 4.45 Å, b = 4.37Å and c = 2.90 Å) close to the [0 0 1] zone axis. The FFT (figure 4(*b*)) from a portion of the crystal shows a near square pattern indicative of this zone in which the lattice parameters a and b are nearly equal. In this zone, the (1 0 0) and (0 1 0) reflections are present due to double diffraction (figure 4(*b*) in red). The corresponding IFFT image shows the lattice spacing of (1 0 0) and (0 1 0) is ~4.4Å. Such HRTEM analyses confirm that the carbide nanoparticles have an acicular morphology with the aspect ratio varying between phases and preparation conditions from 2 : 1 to 7 : 1, and the crystallites are surrounded by a thin graphite-like layer. Due to limited particle imaging statistics, it remains unclear whether the particles exist as individual Co_3C and Co_2C phases or as an admixture of the two phases within individual particles.

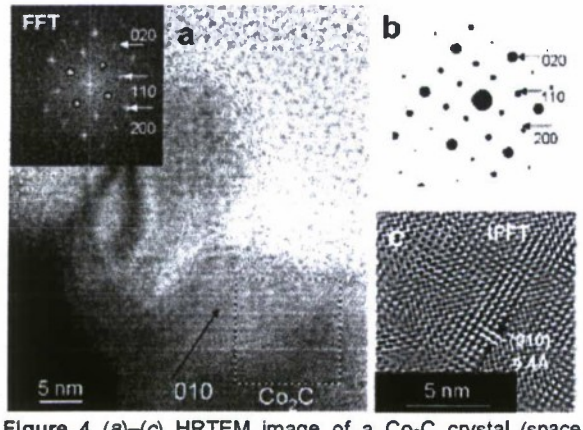

Figure 4 (*a*)–(*c*) HRTEM image of a Co_2C crystal (space group: *Pnnm* with a = 4.45 Å, b = 4.37Å and c = 2.90 Å) close to the [0 0 1] zone axis. The FFT (*b*) from a portion of the crystal shows a near-square pattern indicative of this zone in which the lattice parameters, a and b, are nearly equal. The (1 0 0) and (0 1 0) reflections are present due to double diffraction (*b*) in red. The IFFT image indicates the lattice spacing of (1 0 0) and (0 1 0) is ~4.4Å. (Color online.)

Table 1 presents the phase volume ratios and lattice parameters of each phase determined by Rietveld reduction analyses of the XRD data for several samples. In addition to these data derived from XRD analyses, similar data from selected area electron diffraction (SAED) as well as values reported in the literature from bulk standards are presented [31]. The XRD and SAED determined lattice parameters are consistent with bulk values within the uncertainty of the measurements and analyses.

Figure 5 is a room temperature hysteresis loop curve of one cobalt carbide nanoparticle sample. For this sample the room temperature magnetization under an applied field of ~17 kOe is 73 emu g^{-1} with a coercivity of 3.1 kOe. For the purposes of this study we report the magnetization at 17 kOe as the saturation magnetization (M_s) although it is clear that complete saturation was not attained. This sample has a room temperature $(BH)_{max}$ of 20.7 kJm^{-3}. All magnetization values have been corrected for the presence of the nonmagnetic graphitic surface layer. The correction involved the calculation of the surface layer

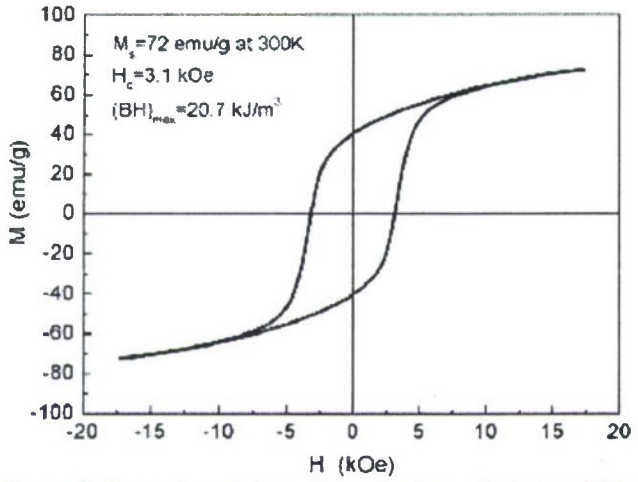

Figure 5 Room temperature hysteresis loop of representative sample having *Ms* of 73 emu g−1 and an *Hc* of 3.1 kOe. The *(*BH*)*max is 20.7 kJm^{-3}.

volume based upon the thickness measured in HRTEM images and assuming a rectangular cross section leading to the renormalization of the magnetic moment. Figure 6 presents the room temperature saturation magnetization and coercivity data for many Co_xC particle samples collected over the course of this study. There exists a significant variation of properties coinciding with a broad range of chemical process parameters. However, it is clear from figure 6 that there is a trade-off in magnetic properties, that is, the greater the saturation magnetization the lower the coercivity. We have found that these magnetic properties can be controlled by careful selection of process parameters and coincide with variations in the Co_2C:Co_3C volume fraction and relative particle size and morphology of each phase. The error bars presented on the data points in figure 6 represent the uncertainty in the measurement of saturation magnetization due to the ambiguity in volume and mass of the particle sample.

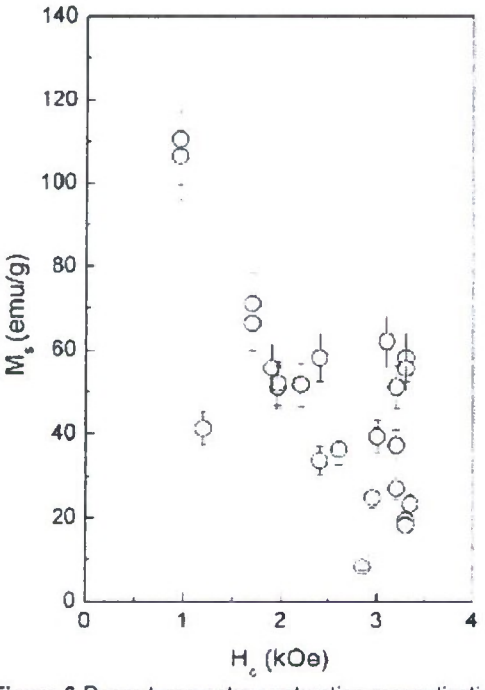

Figure 6 Room temperature saturation magnetization (*Ms*) and coercive field (*Hc*) data for many particle samples collected over the course of this study. Saturation magnetization values correspond to moments measured under the application of 17 kOe.

Figure 7 is a plot illustrating the interrelationship between saturation magnetization and coercivity to the volume fraction of Co_2C toCo_3Cmeasured by XRD (see Table 1). One sees that as the relative fraction of Co_2C increases the magnetization reduces while concomitantly the coercivity increases. Error bars reflect the measurement uncertainty. These results suggest the role of each carbide phase. For example, the Co_3C appears to be largely responsible for the samples saturation magnetization while the Co_2C is responsible for the coercivity. It does not, however, indicate the fundamental origin of the room temperature coercivity measured in these samples. Since the particles are clearly acicular in morphology one can conclude that dipolar or shape anisotropy is responsible for some fraction of the coercivity. Further, the atomic structure in these phases deviates from cubic symmetry and therefore a second source of anisotropy is expected to be of a magnetocrystalline nature. Other sources of coercivity may be related to exchange between

particles. Such interparticle exchange, including that of Co_2C–Co_2C, Co_2C–Co_3C and Co_3C–Co_3C, may provide yet other significant contributions to anisotropy, and subsequently coercivity, in these nanoparticle carbide systems.

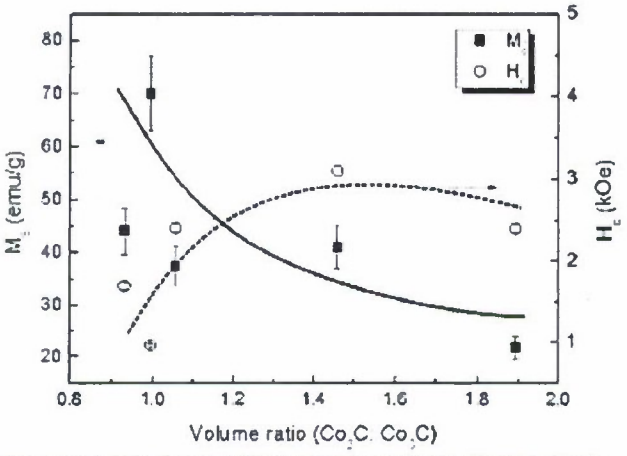

Figure 7 A plot of magnetic properties versus the phase volume ratio illustrating the interrelationship between saturation magnetization and coercivity to the volume fraction of Co2C to Co3C measured by XRD. The plotted line is intended as a guide to the eye. Error bars reflect the uncertainty in measured values.

Thermomagnetic properties of a representative carbide powder sample are presented in figures 8 and 9. Figure 8 illustrates the temperature response of magnetization for a sample heated from 10 to 900 K. Magnetization data were collected as a function of temperature under the application of 0.5 and 10 kOe fields. The data of figure 8, collected under the application of a 10 kOe field, began at 10 K and approached a Curie temperature of ~510 K. The solid curve is a fit to a molecular field approximation. At temperatures approaching 700 K a dramatic increase in magnetization is measured. The thermal cycle reveals an irreversible transformation. The magnetization and high Curie temperature of the sample heated above 700 K is consistent with metallic cobalt. We conjecture that during this vacuum heat treatment the carbide disassociates to metallic cobalt and free carbon. Having a Curie temperature near 510 K, and lacking high temperature chemical and structural stability, these materials may be presently limited to room temperature permanent magnet applications.

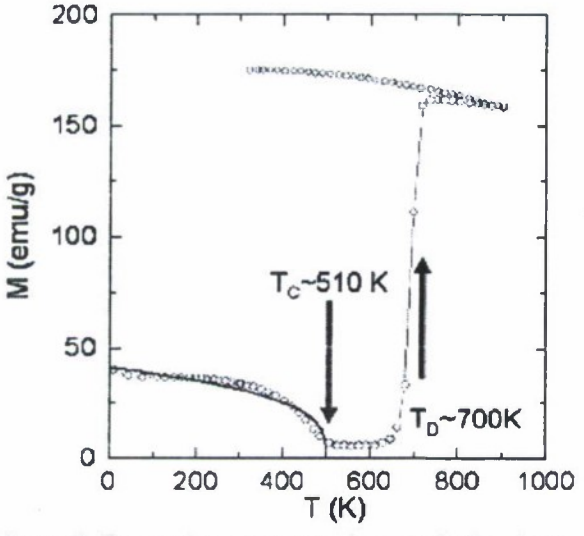

Figure 8 Temperature response of magnetization for a representative sample heated from 10K to over 900 K. The magnetization was collected under the application of a 10 kOe field. The solid curve is a fit to a molecular field theory approximation with TC of 510 K. At temperatures approaching 700K an irreversible transformation occurs. The high magnetization and Curie temperature of the sample heated above 700K is consistent with metallic cobalt.

It has been established that these carbide nanoparticles exist in two phases, namely Co_2C and Co_3C. The room temperature hysteresis loop of figure 5 illustrates a continuous variation of magnetization through remanence; behaviour that is consistent with a single magnetic phase or the exchange coupling of the two carbide phases. Figure 9 contains both 300 and the 10 K hysteresis loops of a representative sample and clarifies this assertion. At 10 K, a knee is observed near remanence indicating the decoupling of hard and soft phases, which originates from profound differences in the temperature dependences of magnetocrystalline anisotropy $K(T)$, magnetization $M(T)$ and exchange constant $A(T)$ between soft and hard phases [32]. From the trends seen in figure 7, the soft phase is likely Co_3C. These

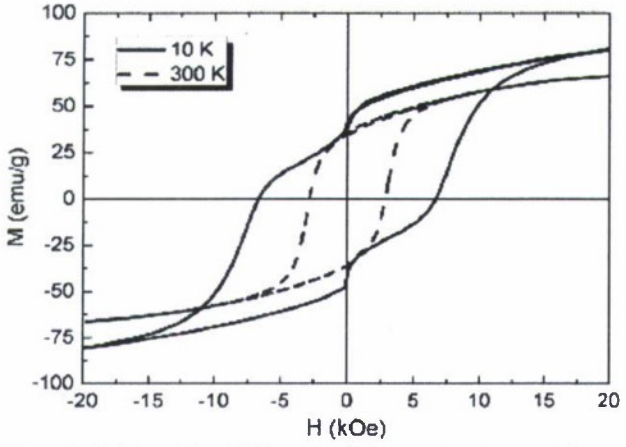

Figure 9 300K and the 10K hysteresis loops of a representative sample. At 10K a knee is observed near remanence indicating the decoupling of hard and soft phases. Results infer that Co_2C and Co_3C phases are exchange coupled at room temperature but not at 10 K.

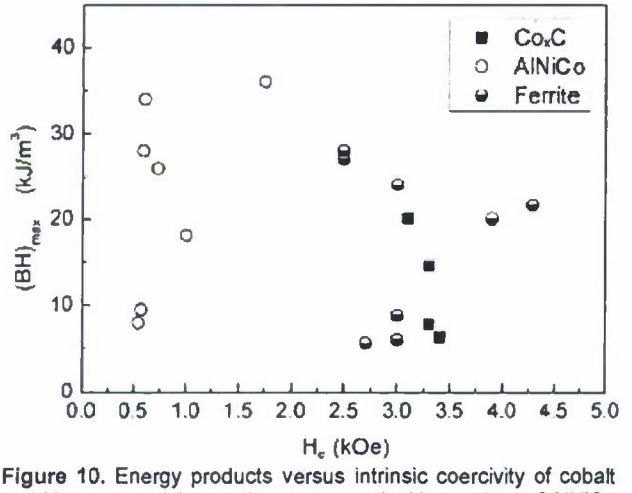

Figure 10. Energy products versus intrinsic coercivity of cobalt carbide nanoparticle powders compared with powders of AlNiCo and ceramic ferrite systems. Vales of (BH)max of Co_xC were calculated with corrected magnetization values. (See text for details.)

results infer that the Co_2C and Co_3C phase are exchange coupled at room temperature. Whether the exchange is of a particle– particle nature, or as an admixture of the two phases, is as yet unknown. Figure 10 displays a comparison of $(BH)_{max}$ versus H_c among Co_xC, AlNiCo and Ba/Sr ferrite magnets. AlNiCo is shown to exhibit high $(BH)_{max}$, 35 kJm^{-3}, but a low intrinsic coercivity, mostly <1 kOe, whereas Ba/Sr ferrite features high intrinsic coercivity, 3–4.5 kOe, but typical values of $(BH)_{max}$ below 25 kJm^{-3}. However, the multiple-phase cobalt carbide nanoparticles demonstrate noticeable characters of permanent magnets, i.e. H_c ~3.5 kOe and $(BH)_{max}$ ~20 kJm^{-3}. This system has the potential to compete with both ferrites and AlNiCo; the ferrite market segment in particular is second only to Nd–Fe–B. To date, the study of cobalt carbide particles is limited to the results presented here. Due to surface dead layers and nanomagnetic surface coatings, one would expect an increase in magnetization for larger Co_xC particles. Therefore, it is expected that higher $(BH)_{max}$ may be achieved in carbide permanent magnets with optimization of size, shape and volumetric ratio of the two phases.

References

1. A. M. Ghemawat, M. Foldeaki, R. A. Dunlap R A, and R. C. O'Hadley, IEEE Trans. Magn. **25**, 3312 (1989).
2. G. Hadjipanayis, J. Liu, A. Gabay, and M. Marinescu, J. Iron Steel Res. Int. **13**, 12 (2006).
3. H. Zijlstra, in Ferromagnetic Materials, edited by E. P. Wohlfarth (North-Holland, Amsterdam, 1980), Vol. 3, p. 37.
4. K. J. Strnat, in Ferromagnetic Materials, edited by E. P. Wohlfarth (North-Holland, Amsterdam, 1980), Vol. 4, p. 131.
5. S. A. Majetich and E. M. Kirkpatrick, IEEE Trans. Magn. **33**, 3721 (1997).
6. J. Ding, P. G. McCormick, and R. Street, J. Alloys Compd. **228**, 102 (1995).
7. H. Zheng, J. Li, J. P. Liu, Z. L. Wang, and S. Sun, Nature (London) **420**, 395 (2002).

8. J. Zhang, Y. K. Takahashi, R. Gopalan, and K. Hono, J. Magn. Magn. Mater. **310**, 1 (2007).
9. E. M. Kirkpatrick, S. A. Majetich, and M. E. McHenry, IEEE Trans. Magn. **32**, 4502 (1996).
10. O. Gutfleisch, M. Kubis, A. Handstein, K.-H. Müller, and L. Schultz, Appl. Phys. Lett. **73**, 3001 (1998).
11. Y. Wang, Y. Li, C. Rong, and J. P. Liu, Nanotechnology **18**, 465701 (2007).
12. R. L. Schalek, D. L. Pelecky, J. Knight, D. J. Sellmyer, and S. C. Axtell, IEEE Trans. Magn. **31**, 3772 (1995).
13. E. Alff, D. Givord, and J. P. Haberer, IEEE Trans. Magn. **9**, 631 (1973).
14. M. A. Willard, L. K. Kurihara, E. E. Carpenter, S. Calvin, and V. G. Harris, Int. Mater. Rev. **49**, 125 (2004).
15. H. W. Gu, B. Xu, J. C. Rao, R. K. Zheng, X. X. Zhang, K. K. Fung, and C. Y. C. Wong, J. Appl. Phys. **93**, 7589 (2003).
16. Y. Hou, Z. Xu, S. Peng, C. Rong, J. P. Liu, and S. Sun, Adv. Mater. (Weinheim, Ger.) **19**, 3349 (2007).
17. R. Skomski and J. M. D. Coey, Phys. Rev. B **48**, 15812 (1993).
18. E. F. Kneller and R. Hawig, IEEE Trans. Magn. **27**, 3588 (1991).
19. Z. H. Wang, C. J. Choi, B. K. Kim, J. C. Kim, and Z. D. Zhang, Carbon **41**, 1751 (2003).
20. Y. H. Lee, Y. S. Huang, J. F. Min, G. M. Wu, and L. Horn, J. Magn. Magn. Mater. **310** 913, (2007).
21. T. J. Konno, K. Shoji, K. Sumiyama, and K. Suzuki, J. Magn. Magn. Mater. **195**, 9 (1999).
22. H. Wang, S. P. Wong, W. Y. Cheung, N. Ke, W. F. Lau, M. F. Chiah and X. X. Zhang, Mater. Sci. Eng. C **16**, 147 (2001).
23. F. H. Zeng and X. Zhang, J. Magn. Magn. Mater. **309**, 160 (2007).
24. S. J. Black, C. P. Morley, A. E. Owen, and M. R. Elsegood, J. Organomet. Chem. **689**, 2103 (2004).
25. P. A. Premkumar, A. Turchanin and N. Bahlawane, Chem. Mater. **19**, 6206 (2007).
26. M. E. McHenry, S. A. Majetich, J. O. Artman, M. DeGraef, and S. W. Staley, Phys. Rev. B **49**, 11358 (1994).
27. Z. X. Zhang, B. B. Cao, and H. M. Duan, J. Mol. Struct.: Theochem **863**, 22 (2008).
28. C. N. Chinnasamy, J. Y. Huang, L. H. Lewis, B. Latha, C. Vittoria, and V. G. Harris Appl. Phys. Lett. **93**, 032505 (2008).
29. T. Matsushita, T. Iwamoto, M. Inokuchi, and N. Toshima, Nanotechnology **21**, 095603 (2010).
30. S. H. Huh and A. Nakajima, J. Appl. Phys. **99**, 064302 (2006).
31. J. Clarke, Chem. Ind. (Lond.) **46**, 1004 (1951).
32. L. Withanawasam, A. S. Murthy, and G. C. Hadjipanayis, IEEE Trans. Magn. **31**, 3608 (1995).

Navy impact

The production and characterization of permanent magnets with an energy product of $(BH)_{max}$ ~20 kJm^{-3} based upon nanoscale cobalt carbide particles that provide a rare-earth free alternative to high performance permanent magnets has been

demonstrated in this program. The cobalt carbide-based magnets described herein are processed by chemical polyol reduction of metal salts. The precipitate of the reaction need only be rinsed and dried prior to packaging. Packaging may be in the form of isotropic or anisotropic high density compacts, bonded magnets, particle suspensions, etc.

Permanent magnet applications of relevance to the Navy include those for directing and shaping particle beams and electromagnetic waves (cathode ray tubes, travelling wave tubes, klystrons, cyclotrons, ion pumps, etc), providing magnetic bias fields for a wide range of RF, microwave and millimeter-wave devices (isolators, circulators, phase shifters, filters, etc), energy conversion (e.g. magnetos, generators, alternators, eddy current brakes, motors and actuators) and exerting attractive and repelling forces (e.g. magnetic separators, latches, torque drives, bearings, etc). Ferromagnetic nanoscale cobalt carbide permanent magnet materials may address the shortcomings of magnets containing rare earth elements that provide the highest energy products, $(BH)_{max}$, but are expensive and prone to corrosion and, as such, pose severe cost limitations as well as supply chain challenges to commercial industries.

Summary

In summary, the magnetic and structural properties of cobalt carbide nanoparticles processed using a single-step polyol reduction reaction were presented. Particles are shown to be acicular in morphology, typically assembled as clusters, with room temperature coercivities in some samples greater than 3.4 kOe and maximum energy products greater than 20 kJm^{-3}. Consisting of Co_3C and Co_2C phases, the ratio of phase volume and particle morphology determine permanent magnet properties. In figure 10 the energy product versus intrinsic coercivity of cobalt carbide nanoparticles is compared with free powders of AlNiCo and ceramic magnets of the Ba/Sr hexaferrite type. Curie temperatures near 510K indicate suitability for room temperature permanent magnet applications; however, at temperatures approaching 700K the carbide particles disassociate irreversibly to carbon and metallic cobalt. The unexpectedly large room temperature coercivities originate from dipolar and magnetocrystalline anisotropies of carbide phases but may be additionally affected by inter-particle exchange. The demonstration of a room temperature energy product greater than 20 kJm^{-3} in nanoparticle cobalt carbides provides a new and viable avenue to realizing rare earth free permanent magnet materials. A complete investigation in which chemical processing parameters are optimized with respect to particle size, phases, chemistry, morphology and packing density (as isotropic and anisotropic compacts) of the cobalt and iron carbide particle systems is likely to result in further enhancement in magnetization, coercivity and Curie temperature.

List of published materials derived from sponsor funding

1. V. G. Harris, Y. Chen, A. Yang, S. Yoon, Z. Chen, A. L. Geiler, J. Gao, C. N. Chinnasamy, L. H. Lewis, C. Vittoria, E. E. Carpenter, K. J. Carroll, R. Goswami, M. A. Willard, L. Kurihara, M. Gjoka, and O. Kalogirou, "High Coercivity Cobalt Carbide Nanoparticles Processed via Polyol Reaction: a New Permanent Magnetic Material," J. Phys. D 43, 165003 (2010).

2. C. N. Chinnasamy, J. Y. Huang, L. H. Lewis, B. Latha, C. Vittoria, and V. G. Harris, "Direct chemical synthesis of high coercivity air-stable SmCo nanoblades," Appl. Phys. Lett. **93**, 032505 (2008).